SCIREA Journal of Electrical Engineering
ISSN: 2995-7141
http://www.scirea.org/journal/DEE
March 11, 2026
Volume 11, Issue 1, February 2026
https://doi.org/10.54647/dee470576

Mathematical Modeling and Analysis of Vibration Reduction of a Simulated Femoral Shaft using Robotic Assisted Damping Drilling System

Orelaja Oluseyi.A[1*] , Odunlami Samson.A[2], Xingsong Wang[3], Adeleke M.B[1]

[1] School Department of Mechanical Engineering, Moshood Abiola Polytechnic, Abeokuta, Nigeria

[2] School Department of Mechanical Engineering, Fededral Polytechnic Ilaro, Ogun State, Nigeria

[3] School Department of Electro-Mechanical Engineering, Southeast University, Nanjing, China

***Corresponding Author:** orhesheywal@yahoo.com (Orelaja Oluseyi.A)

Abstract

Femoral shaft fracture is one of the prominent high impact energy injuries of the lower extremity. One of the common techniques to cut hard tissues in orthopedics, neurosurgery, and others is drilling. Robot assisted femoral shaft drilling and fracture reduction systems have been designed and their applications in the theatre room are vast, but still have some demerits. The use of robots in the theatre room for drilling and cutting hard tissues are so enormous due its flexibility and high precision Although, vibration drilling is also a method of adding axial vibration to the drill bit, but the objective research work is to focus on the modeling and analysis of possible damage caused by high cutting force and vibration with an effort to reduce the drilling force and the consequence of vibration on bone micro-structure during

repositioning and drilling. This experiment encompasses the use of integrated vibration reduction system includes ‘8 sets of visco-elastic air balloon damper’, 6DOF Hans Robot, flexible bracket, contact vibration sensor, force sensor, the jig frame, the drill, air-pump, proportional air controller (PAC), air control lines, drill, speed controller, voltage amplifier and Monitor (Laptop).

Keywords: Drilling, Vibration, Reduction, Force, Muscle, Femur, Analysis, Signal Processing

1.0 Introduction

Minimally invasive techniques such as surgical drilling offer clear advantages in fracture management, including smaller incisions, reduced blood loss, and faster recovery times [1, 2]. Biological osteosynthesis remains the most widely adopted method, providing shorter surgical duration, quicker healing, and fewer complications compared to traditional anatomic reconstruction. For displaced femoral fractures, closed intramedullary (IM) nailing is considered the gold standard, as it preserves anatomical alignment and creates a favorable mechanical environment for bone healing.

Fracture repair relies heavily on accurate repositioning, reduction, and drilling of bone fragments. However, conventional IM fixation often requires radiographic monitoring, exposing both patients and medical staff to significant radiation. Surgeons also face ergonomic challenges, including musculoskeletal strain and long-term occupational risks. Traditional manual techniques further increase the likelihood of soft-tissue injury and complications due to forceful manipulation during drilling [4, 5]. Robotic-assisted systems have emerged as promising alternatives, offering precision and flexibility in orthopedic procedures. Yet, challenges remain-particularly excessive vibration and cutting forces during drilling, which can damage bone microstructure and compromise outcomes [7–9]. Since bone properties change with fracture and density variations, vibration control is critical to ensure safety, reduce operative time, and optimize drilling performance [10, 11].

To address these limitations, we developed a robot-assisted drilling system with integrated force and vibration reduction mechanism susing a femoral shaft bone model that replicates human musculoskeletal characteristics, this system enables surgeons to practice vibration-controlled drilling. The incorporation of a soft air-controlled damper demonstrates effective

vibration reduction, bridging gaps in previous research and offering promising clinical applicability. Ultimately, this approach enhances surgical precision, minimizes complications, and improves patient outcomes in femoral shaft fracture repair.

2.0 Methodology

2.1 Apparatus for intraoperative control of force, torque and vibration reduction system

In order to ascertain the viability of this control and reduction technique used, two sets of experiments were conducted under different speeds, with varying drilling force and balloon pressures. The simulated human bone and muscles used for this experiment has a very similar physical and materials characteristic of real human bone and muscles. The muscles are made up of flexible rubber tube and silicone, since silicone has similar appearance to human body, especially in terms of stiffness [12, 13]. In order to experimentally illustrate force, torque control and vibration reduction caused by the dynamic components of the cutting force, another important parameter gives some vital idea about the relative position between the drill and the femur bone. The bone-tissue vibration effect was measured by contact displacement sensor (CDS), while the balloon pressure differences are controlled by the proportional air controller (PAC). The reduction in frequency of vibration of the bone and analysis of the drill is then observed, however, the equation of the dynamic response of the bone during cutting can be formulated**:**

$$[\mathrm{M}]\begin{Bmatrix}\ddot{X}_b\\ \ddot{Y}_b\\ \ddot{Z}_b\\ \ddot{\Theta}_b\end{Bmatrix}+[\mathrm{C}]\begin{Bmatrix}\dot{X}_b\\ \dot{Y}_b\\ \dot{Z}_b\\ \dot{\Theta}_b\end{Bmatrix}+[\mathrm{K}]\begin{Bmatrix}X_b\\ Y_b\\ Z_b\\ \Theta_b\end{Bmatrix}=\begin{Bmatrix}F_x(t)\\ F_y(t)\\ F_z(t)\\ T_b(t)\end{Bmatrix} \quad (1)$$

Where M denotes the lumped mass, C is the damping coefficient and K is the stiffness matrices of the model femur, andx_b(t) andy_b(t) represent the lateral and axial forces, while z_b (t), and θ_b(t) are the torsional deflections of the femur in the global coordinate system as suggested by [14, 15] . Also, the amount of deformations caused by drilling forces acting on the bone while drilling areF_x(t),F_z (t) which are the lateral forces and F_y(t) which is the thrust force, with torque being denoted as T_b (t).The schematic diagram in Figure 1 showing the force and vibration reduction method set-up using automated air controller embedded with soft air damper. The entire set-up include a soft damper clamp well designed and manufactured for this purpose, the compressed air source for the reduction process is from the

air pump output supplied to the concentric balloon placed round the already re-positioned, implanted and IM nailed fractured bone as shown in Figure 1.0

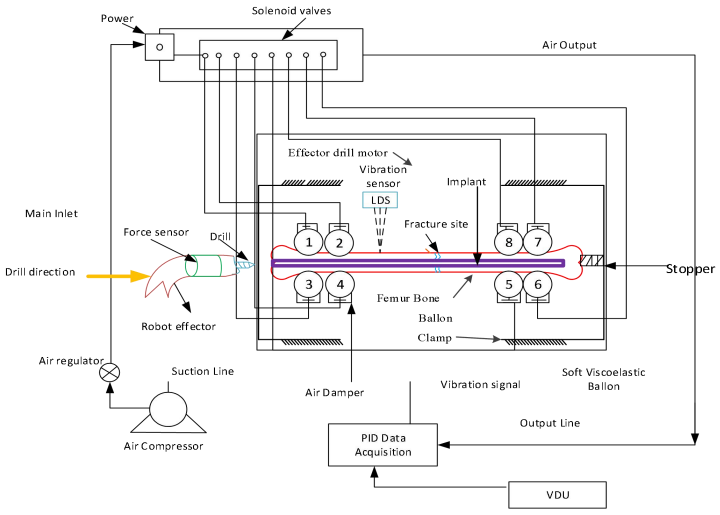

Figure 1 Showing the schematic diagram of drilling force and vibration reduction process during robotic assisted fracture bone repair

In order to reduce high vibration during bone drilling, the initial displacement of the fracture bone was noted and then repositioned by placing it in the concentric of the soft air balloon damper and then increase the balloon pressure to create firmness on the fracture bone, thereby aiding the bone alignment. However, with a considerable increase in the balloon pressure, the drilling force and vibration were measured by the force sensor coupled to the robot manipulator and the contact displacement sensor (CDS) to measure the displacement caused to the bone during this drilling process. The pictorial view is shown in Figure 2 (a and b) below.

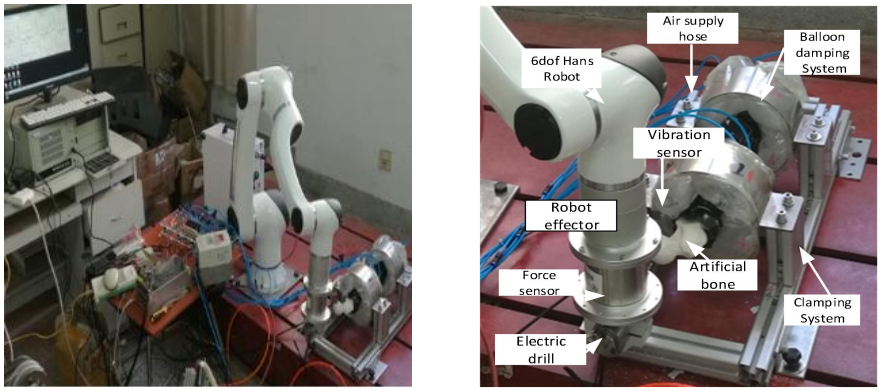

(a) (b)

Figure 2 (a and b) Showing the experimental set-up for force, torque control and vibration reduction during femur bone drilling process

2.1 Design of a data acquisition system

The integrated vibration reduction system includes '8 sets of viscoelastic air balloon damper', 6DOF Hans Robot, flexible bracket, contact vibration sensor, force sensor, the jig frame, the drill, air-pump, proportional air controller (PAC), air control lines, drill, speed controller, voltage amplifier and Monitor (Laptop). The data acquisition connection set-up for this experiment is shown in Figure 3. The force sensor measures the drilling force and torque applied along the x, y, and z-axis, while the contact displacement (CDS) sensor measures the resulted vibration along x, y, and z-axis respectively. All the acquisition signals from the sensors arrangement provides the core module of our force, torque measurement, control and vibration reduction system; we employed well grooved and evenly distributed architecture to ensure reliability and quality of our data, especially on the regulation of the balloon pressure [21] . Data acquisition and management were controlled using (Matlab 16b) with data saved in text files for post-processing analysis. The data were analyzed with the aim of measuring and controlling forces, torques and observing the reduction of vibration during the surgical drilling of femur bone.

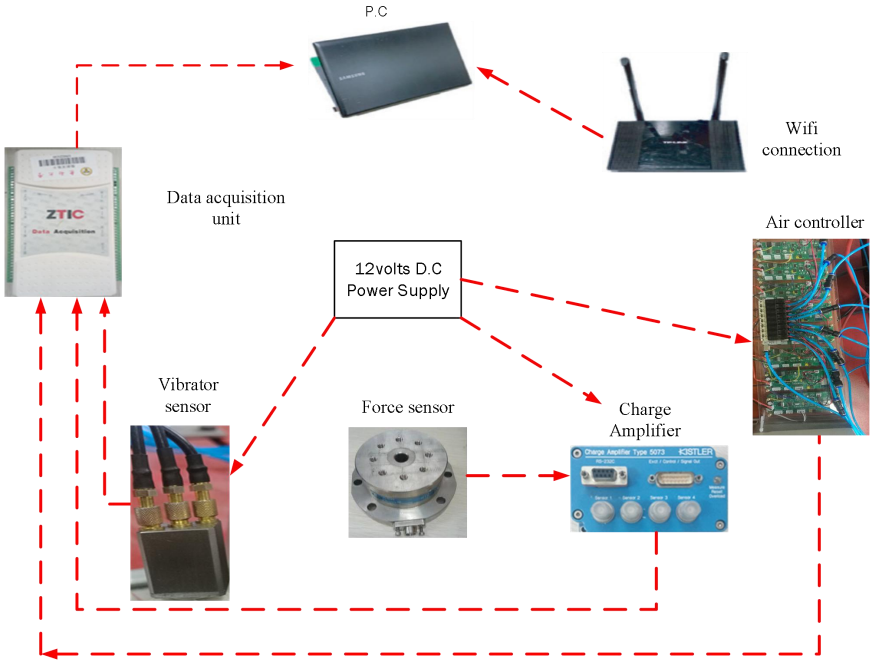

Figure 3 Force Measurement and Vibration reduction Data Acquisition System

The set-up shown in Figure 4 (a and b) illustrate the experimental set up of both un-damped and damped robotic assisted femoral shaft drilling for a better clarification, however, the modeling of this drilling process is also shown in Figure 5 for a mathematical analysis.

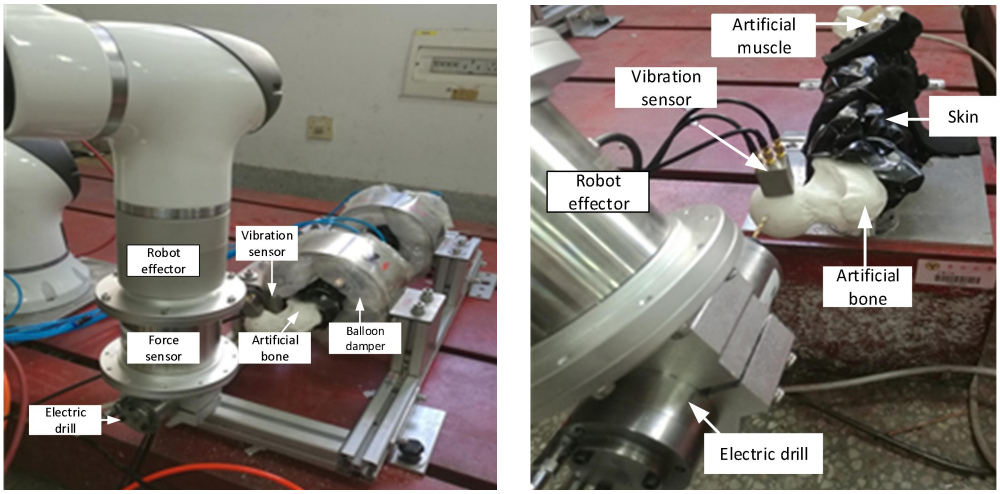

(a) (b)

Figure 4(a and b) Showing balloon damped and un-damped vibration during robotic assisted femur bone drilling process

2.2 Mathematical Modeling of Vibration Absorber System

(a) A general 2DOF vibrating system of a femoral shaft

The dynamic vibration absorber system (DVAS) to be applied to surgical bone drilling is proposed in our experimental procedure, the set-up is presented as 2DOF vibrating system. Although this concept has never been applied in the area of surgical research in the past years, it involves the use of 2DOF air damped balloon dynamic vibration absorber model (BDVAM) for bone drilling, this studied is shown in Figure 6, the mass ratio (μ)i.e the ratio of the femur shaft to m_2 *to* the auxiliary mass m_1 (frame) it is always assumed to be greater than unity ($\mu >>1$), where (ζ) is the damping ratio, two cases are presented in our study.

CASE 1: General application of damping in bone drilling

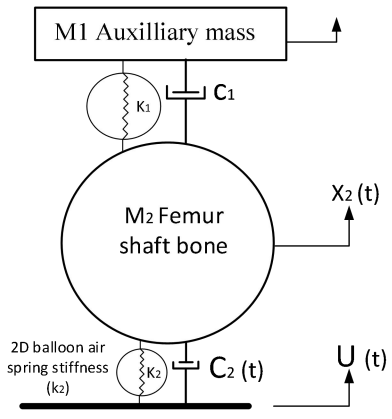

Figure 5 A general 2DOF vibrating system of a femoral shaft (BDVAM) ($\mu >>1$).

The equation of motion of general 2DOF of a femoral shaft in case 1 is represented by;

$$m_1\ddot{x}_2 = -k_1(\dot{x}_1-\dot{x}_2)-c_1(\dot{x}_1-\dot{x}_2)-k_2(x_2-u)-c_2(\dot{x}_2-\dot{u}) \quad (4)$$

$$m_1\ddot{x}_2 = -k_1(\dot{x}_1-\dot{x}_2)-c_1(\dot{x}_1-\dot{x}_2) \quad (5)$$

The effect of the air pressure damping ratio on the transmissibility of the vibration on the femoral shaft can then be;

$$Mt_2=\frac{X_2}{U}=\left[\frac{[A_{22}\lambda^2+A_{00}]^2+[A_{11}\lambda]^2}{[B_4\lambda^4-B_2\lambda^2+B_0]^2+[-B_3\lambda^3+B_1\lambda^1]^2}\right]^{\frac{1}{2}} \quad (6)$$

$$Mt_1=\frac{X_1}{U}=\left[\frac{[-A_2\lambda^2+A_0]^2+[A_1\lambda]^2}{[B_4\lambda^4-B_2\lambda^2+B_0]^2+[-B_3\lambda^3+B_1\lambda^1]^2}\right]^{\frac{1}{2}} \quad (7)$$

Where; $A_{22}=2\zeta_2$, $A_{11}=v^2+4\zeta_1\zeta_{2v}$, $A_{00}=2(\zeta_1v^2+\zeta_2v^1)$, and $A_2=4\zeta_1\zeta_{2v}$, $A_1=2\zeta_1v^2$, $A_0=v^2$, and $B_4=1$, $B_3=2\left(\zeta_1+\left({}^{\zeta_1}/_{\mu}\right)+\zeta_2v\right)$, $B_2=(1+\left({}^{1}/_{\mu}\right)+v^2)$, $B_1=2(v\zeta_2+\zeta_1v^2)$, $B_0=v^2$.

(b) Vigot Modeling System as Applied to Surgical Bone drilling of a femoral shaft

2DOF Air damped vibrating system using a balloon air damper (Vigot Model), with system damping coefficients c_1 , c_2 and balloon air damper characteristics i) air damping ratio ζ_a and ii) is the assumed latex balloon which is modeled as 2D air spring rate ratio $k = {}^{k_a}/_{k_1}$, where k_1= 2D balloon air spring stiffness of auxiliary spring and k_a= 2D stiffness of air balloon damper as illustrated in Figure 5.

CASE 2: Vigot Damping Model as Applied to Surgical Bone Drilling

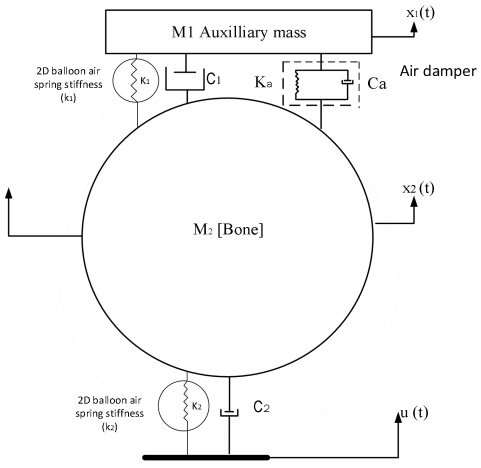

Figure 6 2DOF air damped vibrating system using a balloon air damper (Vigot Model) (Balloon Dynamic Vibration Absorber Model). μ >>1.

The equation of motion using Vigot model for 2DOF of a femoral shaft is represented by;

$$m_1\ddot{x}_2 = -k_1(k_1-k_a)(x_2-x_1)-(c_1-c_a)-c_2(\dot{x}_2-\dot{x}_1)-k_2(x_2-u)-c_2(\dot{x}_2-\dot{u}) \quad (8)$$

$$m_1\ddot{x}_1 = = -(k_1+k_a)(x_2-x_1) - (c_1+c_a)(\dot{x}_2-\dot{x}_1) \quad (9)$$

The effect of the balloon air pressure damping ratio on the transmissibility of the vibration on the femoral shaft can then be;

$$Mt_2=\frac{X_2}{U}=\left[\frac{[-a_{22}\lambda^2+a_{00}]^2+[a_{11}\lambda]^2}{[b_4\lambda^4-b_2\lambda^2+b_0]^2+[-b_3\lambda^3+b_1\lambda^1]^2}\right]^{\frac{1}{2}}= \quad (10)$$

$$= Mt_1=\frac{X_1}{U}=\left[\frac{[-a_2\lambda^2+a_0]^2+[a_1\lambda]^2}{[b_4\lambda^4-b\lambda^2+B_0]^2+[-b_3\lambda^3+b_1\lambda^1]^2}\right]^{\frac{1}{2}} \quad (11)$$

Where; $a_{22}=2\zeta_{2,}a_{11}=v^2+4\zeta_1\zeta_{2v}+4\zeta_a k^{0.5}\zeta_{2v}$, $a_{00}=2(\zeta_1 v^2 + \zeta_2 v^1)$, and$a_2=(4\zeta_1\zeta_{2v}+4\zeta_2\zeta_a k^{0.5}v)$, $a_1=2(\zeta_1 v^2+\zeta_a k^{0.5}v^2+\zeta_{2,}v+k\zeta_2 v)$, $a_0=v^2(1+k)$, and

$b_4 =1$, $b_3=2\left(\zeta_1+\left(\zeta_1/\mu\right)+\zeta_2 v+\zeta_a^{[k^{0.5}+\frac{k^{0.5}}{u}]}\right)$, $b_2=(1+k+4\zeta_1 v\zeta_2+4\zeta_a k^{0.5}v\zeta_2+\left(1/\mu\right)+v^2+(\frac{k}{u})$), $b_1=2(\zeta_2 v+kv\zeta_2+\zeta_1 v^2+\zeta_a k^{0.5}v^2)$, $b_0= v^2(1+k)$,

Assuming while drilling, the femur bone gives rise to a harmonically varying force which is;

$$\mathrm{F}\ (\mathrm{t}) = F_0 cos\omega t \quad (12)$$

Then, following the ideal equation of motion of the drilling force on the bone while is given as;

$$m\ddot{x}+c\dot{x}+kx= F_0 cos\omega t \quad (13)$$

The steady state solution of this equation can be given as;

$$\mathrm{x(t)} = (\mathrm{X}\ cos\omega t - \phi) \quad (14)$$

Where; F_0 is the drilling force, ω is the spindle frequency , and X is the possible static deflection of the bone while drilling.

$$\mathrm{X}=\frac{F_0}{[\left((k-m\omega^2\right)^2+\omega^2 c^2]^{\frac{1}{2}}} \quad (15)$$

And;

$$\phi= tan^{-1}(\frac{\omega_c}{k-m\omega^2}) \quad (16)$$

However, to reduce the vibratory motion on the femur bone, the displacement amplitude of the femur bones mass (M_2) due to the cutting force F(t), given by Equation (16), can be further expressed as:

$$T_d = \frac{X}{\delta_{st}} = \frac{KX}{F_o} = \frac{1}{\sqrt{[(1-r^2)^2+(2\zeta r)^2]}} \tag{17}$$

Where $\frac{X}{\delta_{st}}$ is called, in the present context, the displacement transmissibility or amplitude ratio and it indicates the ratio of the amplitude of the femur bone mass, X, is the static deflection under the constant force F_o [22] .

$$\delta_{st} = \frac{F_o}{k} \tag{18}$$

3.0 Vibration Signal Processing

In this section, the bone vibration signal during drilling process is directly recorded by a contact displacement sensor (CDS), and then a simple method for determining the amplitude of the exact harmonic component signal is proposed.

We assumed that the recorded vibration signal obtained x(t) are made up of several harmonics can then be written as

$$\mathrm{x(t)} = \sum_{i=1}^{L} (\mathrm{X}\ cos\omega t - \phi) \tag{19}$$

Where ϕ is the initial phase angle, since the displacement within the vibration environment sometimes contains impulsive noise, the experimental signal is processed and the window size of the filter is 5. We decide to use wavelet packet transform (WPT) in this study because it provide good frequency resolution and simultaneously sacrifices its time resolution at low frequencies, which is very good for harmonics analysis, although both short time Fourier transform (SFTT) and Hilbert-Huang transform (HHT) can be employed to analyze vibration signal, but the computational method of WPT is lower to STFT and HHT because it has a fast algorithm. It is also believed that the recorded vibration signal varies with the milling force, so there is a need for compensation for harmonic amplitude estimation when the force changes with time because of the anisotropic property of the bone and the elastic properties of muscles and ligament surrounding the bone. It is assumed that the WPT coefficients in the node (n,0) is x_0(p) is with $\mathrm{p} \in \left[0, \frac{N}{2^n} - 1\right]$, and the output value of the displacement sensor is x_n ,

when the vibration occur as a result of drilling advancement into the bone, the harmonic amplitude is $d_k(p)$, as illustrated in Figure 6, it can be mathematically written as:

$$\grave{d}_k(p) = d_k(p)\frac{x_0(0)-x_n}{x_0(p)-x_n} \quad \text{..... (20)}$$

4.0 Results

The in vitro result obtained from the frequency response from the excitation force caused by drilling to the vibration displacement of the bone while varying cutting speed and balloon pressure was obtained. The displacement is obtained as the integral value of acceleration obtained by accelerometer at a specific measurement point. Each drilling is excited in the x, y, and z direction, but we focused our research on Z direction only. Force is measured at the robot effector spindle end, where the force sensor is attached. Damping effects were expected to increase linearly with increased damper size (contact area) within a determined balloon air pressure value, although, if the balloon pressure is too high, the balloon will become too turgid and may not give adequate damping effect needed. In this experiment two robot spindle cutting speed of 500rpm and 1000rpm were selected with varying balloon pressure of 4bar, 6bar, 8bar and 10 bars.

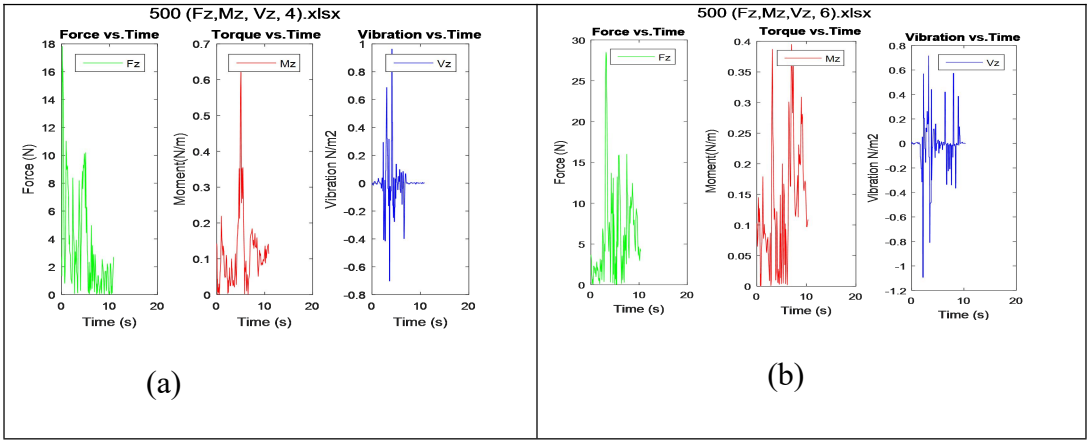

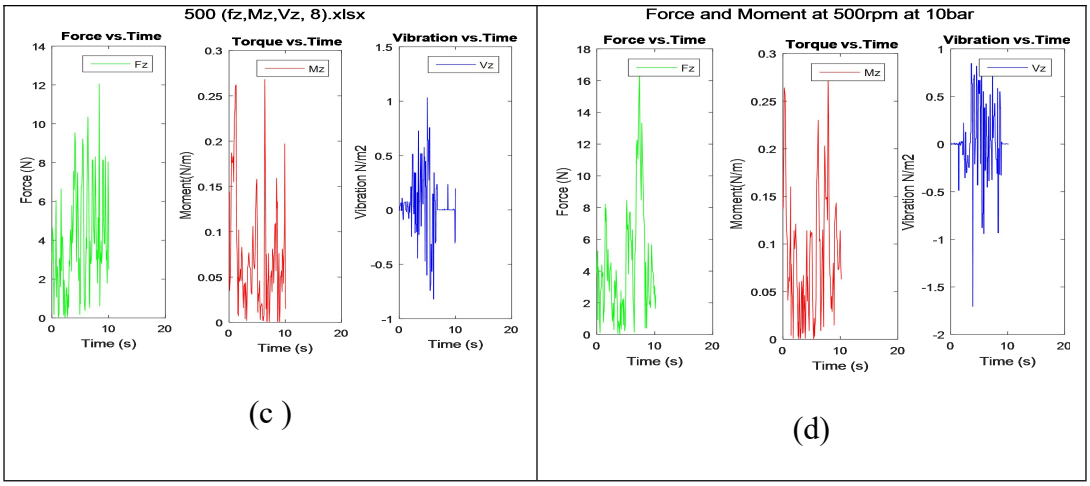

Figure 7 Recorded force, torque control and vibration reduction at 500rpm robot spindle speed with varying pressure of 4bar, 6bar, 8bar and 10bar.

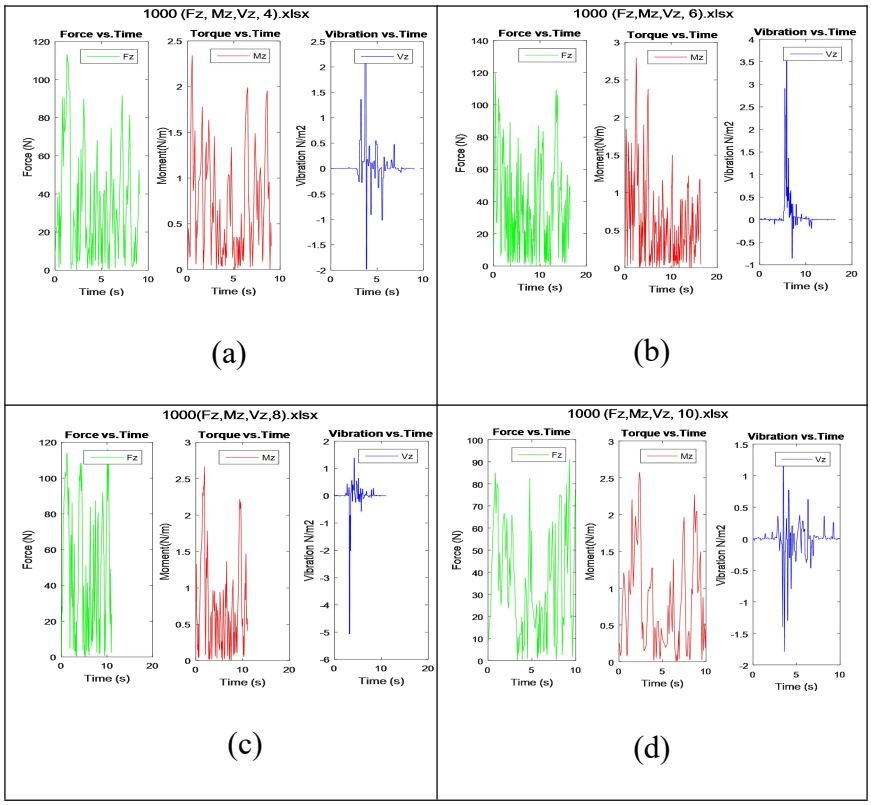

Figure 8 Recorded force, torque control and vibration reduction at 1000rpm robot spindle speed with varying pressure of 4bar, 6bar, 8bar and 10bar.

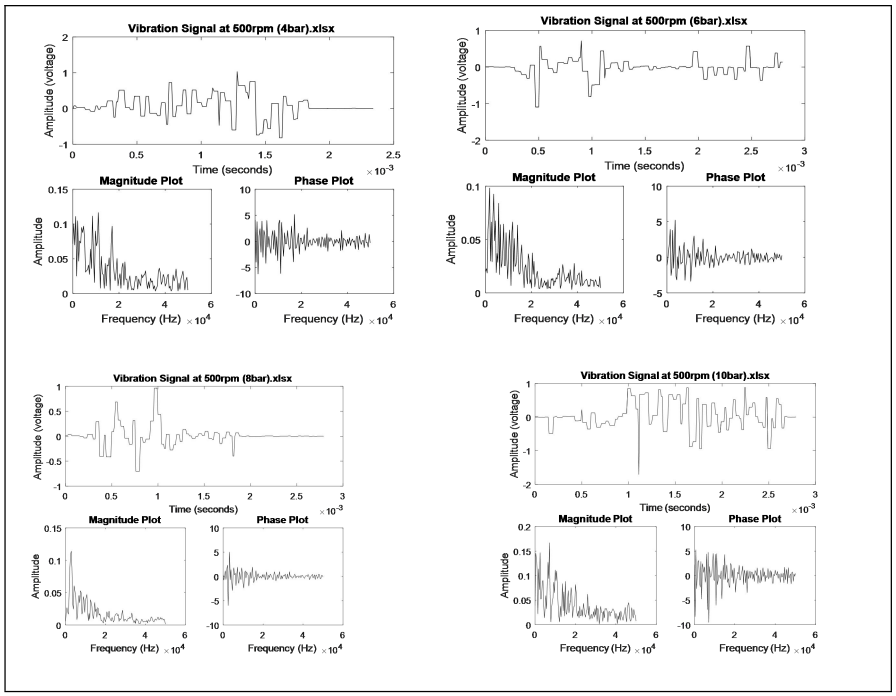

Figure 9 Vibration Filtered SignalAnalysis at 500rpm at 4bar, 6bar, 8bar and 10bar

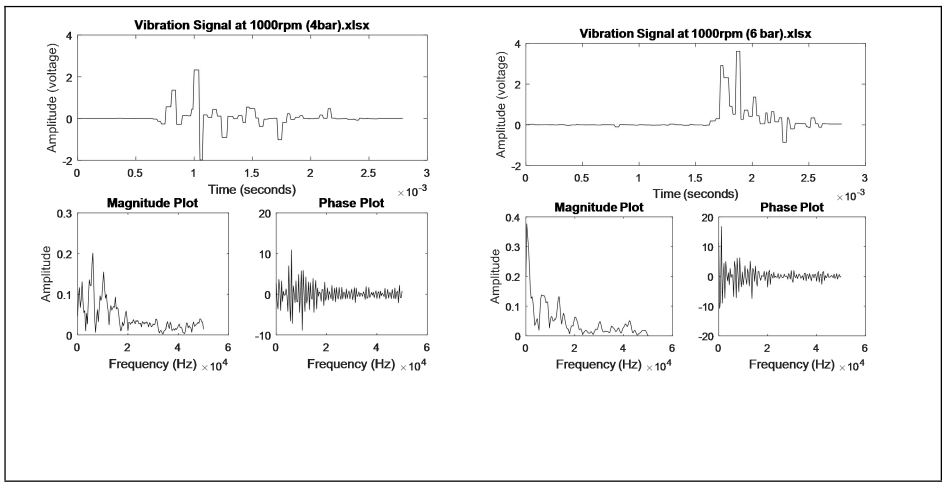

Figure 10 Vibration Filtered Signal Analysis at 1000rpm at 4bar, 6bar, 8bar and 10bar

5.0 Conclusion

In this study the forces and vibrations were measured by force sensor and accelerometer, since in an ideal situation the vibration amplitude of the bone is proportional to the increase in the cutting force, but adequate clamping and damping system minimize the amount of vibration.

Considering that the WPT coefficient in low-frequency suband proportionally reflect the intensity of drilling force, we employed a compensation technique for harmonic amplitude compensation as seen in Figure 7. With the robot spindle speed of 500rpm,it is seen that the drilling forces and torques reduces when the balloon pressure increases from 4bar to 10bar, but a perfect reduction is experienced while the balloon pressure is 8bar, with a very minimal amplitude span and frequency when compared with other balloon pressure result as shown in Figure 8, this can also be seen be seen when the robot spindle drilling speed is increased to 1000rpm, the force, torque and vibration amplitude is minimal at the balloon pressure of 8bar as also shown in Figure 9, as compared with other balloon pressure, this actually shows that at pressure of 8bar, the damping is more effective with less vibration. With further vibration signal processing using FFT and adding more filters, as shown in Figure 10 the vibration signal, the amplitude plot and the phase plot of vibration at spindle speed of 500rpm was further analyzed at the balloon pressure of 4, 6 8 and 10bars to critically show the vibration reduction extent, at the balloon pressure of 4,6 and 10 bar it is seen that the voltage displacement, are lower with balloon pressure of 8bar, considering the magnitude plot and the phase plot in all these three cases, the amplitude voltage span and the frequency of vibration are much lower when the balloon pressure is at 8bar with magnitude plot of range (0 to +0.1) volt, with phase plot range of (+5 to -5) volt with less frequency of vibration. The experimental results verify the correctness of using a soft balloon damper to absorb vibration signal and it is a brilliant concept to control force and torque simultaneously during bone drilling, and this has not been previously applied anywhere in surgical bone drilling. The basic assumptions used in the modeling procedure are based on the geometrical structure of the femur bone and the mechanical properties of a human normal femur bone, it is also important to also know that the individual differences and the clinico-pathologic variances may change the dynamic behavior of a bone. The vibration analysis is based on the preoperative image data obtained.

References

[1] Zhu Q, Liang B, Wang X, Sun X, Wang L. Minimally invasive treatment of displaced femoral shaft fractures with a teleoperated robot-assisted surgical system. J Injury, 2017. 48(10): p. 2253-2259. doi: 10.1016/j.injury.2017.07.014.

[2] Sohn HS, Jeon YS, Lee J, Shin SJ. Clinical comparison between open plating and minimally invasive plate osteosynthesis for displaced proximal humeral fractures: A prospective randomized controlled trial. J Injury, 2017. 48(6): p. 1175-1182. doi: 10.1016/j.injury.2017.03.027.

[3] Cleather DJ, Godwin JE, Bull AM. Hip and Knee joint loading during vertical jumping and push jerking. J. Clin.Biomech (Bristol, Avon), 203. 28(1): p.98-103. doi:1016/j.clinbiomech.2012.10.006.

[4] Oszwald M, Westphal R, Loughlin PF, Kendoff D, Hufner T, Wahl F, Krettek C, Gosling T. A rat model for evaluating physiological responses to femoral shaft fracture reduction using a surgical robot. J Orthopaedic Research, 2008. 26(12):p.1656-9. doi: 10.1002/jor.20698.

[5] Chen W, Jing Y, Lv H, Wang J, Hou Z, Zhang Y. Displaced femoral shaft fractures treated by antegrade nailing with the assistance of an intramedullary reduction device. Inter. J Orthopaedics, 2015. 40(8): p. 1735-1739. doi:10.1007/s00264-015-3036-8.

[6] Bertelsen A, Melo J, Sanchez E, Borro D. A review of surgical robots for spinal interventions. Int J Med. Robotics and Computer Assisted Surgery 2012. 9(4): p. 407-22. doi:10.1002/rcs.1469.

[7] Shweikeh F, Amadio JP, Arnell M, Barnard T, Zachary R, Kim J, Johnson P, Drazin D. Robotics and the spine: a review of current and ongoing applications. J Neurosurgical Focus, 2014. 36(3), E10. doi: 10.3171/2014.1.focus13526.

[8] Ma K, Wang X, Shen D. Design and Experiment of Robotic Belt Grinding System with Constant Grinding Force. Inter. Conf. on Mechatronics and Machine Vision in Practice, 2018. (M2VIP): p. 1-6. doi: 10.1109/m2vip.2018.8600899.

[9] Adamkowski, A., Henke, A., & Lewandowski, M. , Resonance of torsional vibrations of centrifugal pump shafts due to cavitation erosion of pump impellers. J Engineering Failure Analysis, 2016. 70: p. 56-72. doi: 10.1018/j.engfailanal.2016.07.011.

[10] Sun H, Yuan S, Luo Y. Cyclic Spectral Analysis of Vibration Signals for Centrifugal Pump Fault Characterization. IEEE Sensors Journal, 2018.18(7):p.2925-2933. doi:10.1109/jsen.2018.2804908.

[11] Wang Y, Cao M, Zhao Y, Zhou G, Liu W, Li D. Experimental Investigations on Microcracks in Vibrational and Conventional Drilling of Cortical Bone. J Nanomaterials, 2013. p.1-5. doi:10.1155/2013/845205.

[12] Alizad, A., Walch, M. J., Greenleaf, F., and Fatemi, M., Vibrational characteristics of bone fracture and fracture repair: application to excised rat femur. J Biomech Eng, 2006. 128(3): p. 300-8. doi:10.1115/1.2187037.

[13] Zhu, Q., Liang, B., Wang, X., Sun, X., Wang, L., Force-torque intraoperative measurements for femoral shaft fracture reduction. Computer Assisted Surgery, 2016. 21: p. 37-45. doi: 10.1080/24699322.2016.1240311.

[14] Dai Y, Zhang J, Xue Y. Use of wavelet energy for spinal cord vibration analysis during spinal surgery. The Inter J of medical robotics and Computer Assisted surgery, 2012. 9(4): 433-440. doi: 10.1002/rcs.1477.

[15] Coulson, C, Taylor R, Griffiths M, Proops , D, and Brett P. An autonomous surgical robot for drilling a cochleostomy?porcine trial. J Clinical Otolaryngology and Allied Sciences, 2006. 31: p. 580-580. doi: 10.1111/j.1365-2273.2006.01341_6.x.

[16] Lee Y, Park S, Yoon S, Kong Y, Goh J. Pedestrian accident analysis with a silicone dummy block. Inter J Forensic Science, 2012. 220: p. e13-16. doi: 10.1016/j.forsciint.2012.03.001.

[17] Roukema J and Altintas Y. Generalized modeling of drilling vibrations. Part I: Time domain model of drilling kinematics, dynamics and hole formation. International Journal of Machine Tools and Manufacture, 2007.47:p.1455-1473. doi: 10.1016/j.ijmachtools.2006.10.005.

[18] Lee S.J., Liong K, Tse KM, and Lee H.P. Biomechanics of the deformity of septal L-Struts. Laryngoscope, 2010. 120(8): p. 1508-15. doi: 10.1002/lary.20976.

[19] Burr D.B, Turner C.H, Naick P, Forwood M.R, Ambrosius W, Sayeed Hasan M, and Pidaparti R. Does Microdamage Accumulation affect the Mechanical Properties of Bone? J Biomech, 1998. 31(4): p. 337-45.doi: 10.1016/s0021-9290[1]00016-5.

[20] Langer J, Gardner M, Ricci W. The Cortical Step Sign as a Tool for Assessing and Correcting Rotational Deformity in Femoral Shaft Fractures. J Orthopaedic Trauma, 2010. 24: p. 82-8. doi: 10.1097/bot.0b013e3181b66f96.

[21] Fang C, Gibson W, Lau T.M, Fang B, Wong T.M, and Leung F, Important tips and numbers on using the cortical step and diameter difference sign in assessing femoral rotation– Should we abandon the technique?.J.Injury, 2015.46(7).doi: 10.1016/j.injury.2015.04.009.

[22] Füchtmeier B., Egersdoerfer S., Mai R., Hente R., Dragoi D., Monkman G., Nerlich M, Reduction of femoral shaft fractures in vitro by a new developed reduction robot system 'RepoRobo'. J Injury, 2004. 35(1): p. 113-119. doi: 10.1016/j.injury.2004.05.019.